

A Single-Stage High-Frequency Isolated Three-Phase AC/DC Converter

Diego Santos Greff and Ivo Barbi*

*IEEE Senior Member

Federal University of Santa Catarina/Power Electronics Institute
Florianopolis, SC, 88040-970, Brazil
dsgreff@yahoo.com.br, ivobarbi@inep.ufsc.br
http://www.ivobarbi.com

Abstract—Recently global suppliers of telecom energy solutions have been researching alternative rectifier topologies capable of processing high power using ohmic isolation with compact size. This paper introduces a new concept of a single-stage high-frequency isolated three-phase AC/DC converter. In order to validate this topology, forward/flyback converters and three-phase buck rectifiers are briefly reviewed. This paper also presents a modeling and control technique proposal. The theoretical concepts are verified by the digital simulation of a rectifier connected to a $220V_{rms}$ grid delivering $6kVA$ at $60V/100A$.

Keywords - three-phase PWM buck rectifier, high-frequency isolation, dqo transform.

I. INTRODUCTION

The requirements of rigid harmonic standards rule out the use of classic diode rectifiers as the front-end converter for high-power ac-dc applications. These impositions led to the employment of the standard three-phase PWM rectifiers as front-end ac-dc converters, known as boost or buck rectifiers. Both technologies provide low total harmonic distortion, power factor correction, constant power flow, so that minimal filtering component size and cost can be achieved. Buck topologies can be a convenient alternative when the input line voltage is high as opposed to boost topologies, which have the undesirable property of high device voltage ratings, or when the variable dc output voltage exceeds the appropriate levels.

In some high power applications, ohmic isolation between the load and the grid is necessary. In such cases, usually a two-stage power processing unit is used being composed of: a front-end six-switch buck or boost rectifier cascaded with an isolated dc/dc converter. In three-phase uninterruptible power supplies (UPS), isolation is often provided by a bulky commercial frequency transformer either at the input or at the ac output side.

The first high-frequency isolated topology was proposed in the [1] using a switch-mode rectifier (SMR) structure that has six hard switching thyristors with bidirectional current flow. Improvement on this topology [2] can be achieved by using the PWM control method for the SMR, based on coordinate transforms. In this method the iron loss in the transformer may become visible because of the high-frequency.

Reference [3] proposed a novel ZVS PWM three-phase rectifier, topologically equivalent to the converter described

in [1] and [2] but is improved by ZVS which makes use of the parasitic capacitances of the switches and the transformer leakage inductance. However, to obtain all the benefits of this structure, twelve power switches (MOSFETs or IGBTs) and a complicated PWM strategy are required for effective implementation.

In this paper a simple and novel technique to isolate unidirectional three-phase buck rectifiers is introduced. The topology is shown in Figure 1. The high-frequency isolation utilizes a forward/flyback converter introduced by [4]. It is worth emphasizing that no additional switches are required in the dc-dc converter and a wide load voltage regulation is achieved, obviously defined by the transformer design. In order to validate the proposed topology a review of buck rectifiers, the modulation technique used, the modeling and control of the rectifier and simulation results are presented.

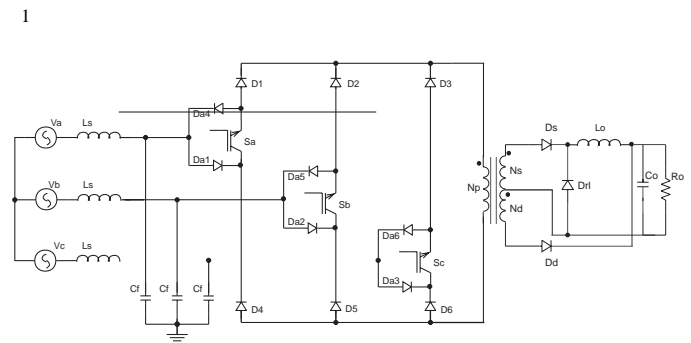


Fig. 1. High-Frequency isolated three-phase AC/DC converter.

II. FORWARD/FLYBACK CONVERTER

High-frequency isolation is achieved by a forward/flyback converter [4], which is actually a forward converter with transformer demagnetization through the load. The forward sub-converter operates in continuous conduction mode (CCM) and the flyback sub-converter in discontinuous conduction mode (DCM). This is defined so that the forward sub-converter processes practically all of the power delivered to the load. Figure 2 shows the topology of the forward/flyback converter.

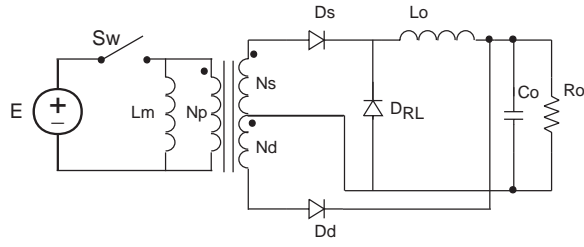


Fig. 2. Forward/flyback converter.

The operating stages can be briefly described in three intervals:

- 1) First Stage: the switch is closed, the transformer's core is magnetized and power is transferred from source E to the load through secondary winding n_s , according to Figure 3(a);
- 2) Second Stage: the switch is opened, the current of L_o free-wheels through D_{RL} , demagnetization of the transformer's core is initiated by the demagnetizing current through demagnetizing winding n_d through the load, as observed in Figure 3(b);
- 3) Third Stage: the switch is still open, the current of L_o free-wheels through D_{RL} and the transformer's core is completely demagnetized, according to Figure 3(c).

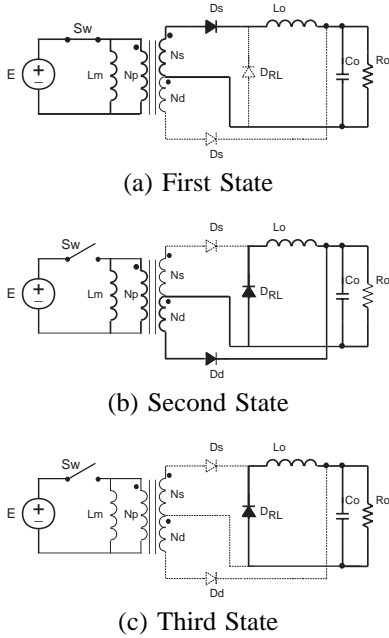


Fig. 3. Operation states of the forward/flyback converter.

Figure 4 shows the main waveforms for the above mentioned operating stages.

From the *volt · second* balance, the ratio of the demagnetizing turns per primary turns is obtained which, ensures the demagnetization of the transformer's core and operation of the flyback sub-converter in DCM.

$$\frac{n_d}{n_p} \leq \frac{V_o}{E} \cdot \frac{(1-D)}{D} \quad (1)$$

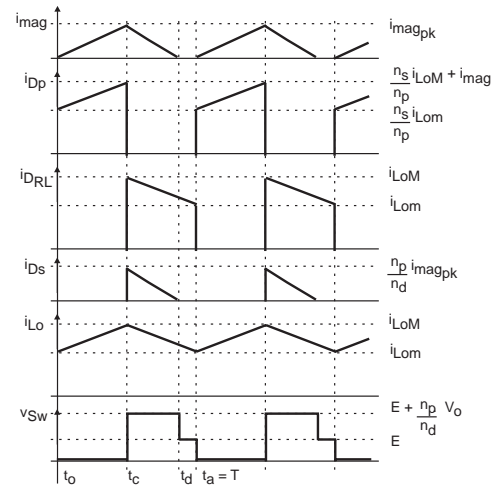


Fig. 4. Forward/flyback converter theoretical waveforms.

As a complement to the operating stages and waveforms, some relevant peak voltage equations can be defined for the semiconductor devices:

Switch peak voltage:

$$v_{swpk} = E + \frac{n_p}{n_d} \cdot V_o \quad (2)$$

Ds secondary diode peak voltage:

$$v_{Dspk} = \frac{n_s}{n_d} \cdot V_o \quad (3)$$

Dd demagnetizing diode peak voltage::

$$v_{Ddpk} = \frac{n_d}{n_p} \cdot E + V_o \quad (4)$$

DRL free-wheel diode peak voltage::

$$v_{Drlpk} = \frac{n_s}{n_p} \cdot V_o \quad (5)$$

III. MODULATION TECHNIQUE

The circuit diagram of the unidirectional three-phase PWM buck rectifier is shown in Figure 1. The use of a unidirectional buck rectifier is justified by the grid-to-load power flow application, simplifying and reducing costs of the power, processing and drive structures [5].

Regarding the line current filtering in the boost topology, the continuous input current minimizes the requirements for additional input filtering, while in the case of the buck rectifier, an input filter is necessary in order to eliminate the switching-frequency harmonics. The buck rectifier operates with a lower output voltage than the boost rectifier. It also presents an advantage when regarding protection since the shoot-through of a bridge leg is possible in the boost rectifier. Therefore, the buck topology could be more convenient in some high power applications.

In classical buck rectifiers a path for the load current must be always available, even at the switching instant. In the proposed topology, it is not appropriate for the switching pattern to provide a continuous path for the load current, since this

TABLE I
MODULATION STATES

State	Two-Level			Three-Level			Switches		
	m_a	m_b	m_c	y_a	y_b	y_c	S1	S2	S3
1	+1	+1	-1	0	+1	-1	1	1	1
2	+1	-1	+1	+1	-1	0	1	1	
3	+1	-1	-1	+1	0	-1	1		1
4	-1	+1	+1	-1	0	+1	1		1
5	-1	+1	-1	-1	+1	0	1	1	
6	-1	-1	+1	0	-1	+1		1	1
0	± 1			0			D_{RL}		

operation would saturate the core of the transformer. Thus, a simplified modulation can be used in this case.

In this paper, a balanced grid voltage source with a peak voltage of V_{pk} :

$$\begin{bmatrix} v_a(t) \\ v_b(t) \\ v_c(t) \end{bmatrix} = \begin{bmatrix} V_{pk} \cdot \sin(\omega \cdot t) \\ V_{pk} \cdot \sin(\omega \cdot t - 120^\circ) \\ V_{pk} \cdot \sin(\omega \cdot t + 120^\circ) \end{bmatrix} \quad (6)$$

Defining three modulating signals $m_a(t), m_b(t), m_c(t)$ with modulation index M :

$$\begin{bmatrix} m_a(t) \\ m_b(t) \\ m_c(t) \end{bmatrix} = \begin{bmatrix} M \cdot \sin(\omega \cdot t) \\ M \cdot \sin(\omega \cdot t - 120^\circ) \\ M \cdot \sin(\omega \cdot t + 120^\circ) \end{bmatrix} \quad (7)$$

A simple way to obtain an adequate scalar modulation is by providing a three-level modulation, as proposed by [6], which applies a transformation matrix to convert a low-level modulated signal into a three-level modulated signal.

$$\begin{bmatrix} y_a(t) \\ y_b(t) \\ y_c(t) \end{bmatrix} = \frac{1}{2} \cdot \begin{bmatrix} 1 & -1 & 0 \\ 0 & 1 & -1 \\ -1 & 0 & 1 \end{bmatrix} \cdot \begin{bmatrix} m_a(t) \\ m_b(t) \\ m_c(t) \end{bmatrix} \quad (8)$$

The matrix of (8) converts the two-level modulating variables $m_a(t), m_b(t), m_c(t)$ into three-level modulating variables $y_a(t), y_b(t), y_c(t)$. The proper magnitude of the modulating signal $y_{abc}(t)$ along with minimum logic implementation can be directly applied to drive the switches.

Table I summarizes the modulating signals and switching states for the modulation presented. In Figure 5, the resulting waveforms of the level transformation illustrate an adequate signal composition to drive the switches of a buck rectifier.

IV. MODELING AND CONTROL

The modeling applied here is based on phase variables in the dqo coordinates system [7], [8], [9]. In order to simplify the analysis, a 90° phase lead is applied to the grid voltage sources (6) and to the modulating signals (7). In the following analysis, the secondary components are transferred to the primary of the transformer.

$$\begin{aligned} R'_o &= \left(\frac{n_p}{n_s}\right)^2 \cdot R_o; L'_o = \left(\frac{n_p}{n_s}\right)^2 \cdot L_o; \\ C'_o &= \left(\frac{n_s}{n_p}\right)^2 \cdot C_o; I'_o = \left(\frac{n_s}{n_p}\right) \cdot I_o; \end{aligned} \quad (9)$$

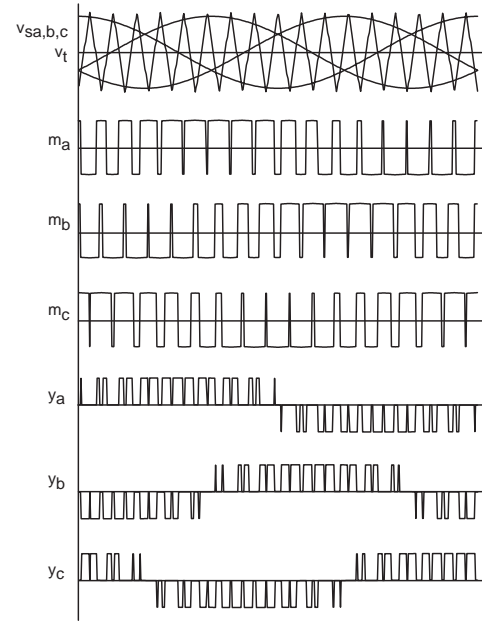


Fig. 5. Transform Waveforms.

A. AC Input Model

The equivalent per phase circuit of the buck rectifier under analysis is shown in Figure 6, and considering that the per phase input current of the rectifier bridge $[i_s(t)]_{abc}$ is defined by:

$$[i_s(t)]_{abc} = I'_o \cdot [m(t)]_{abc} \quad (10)$$

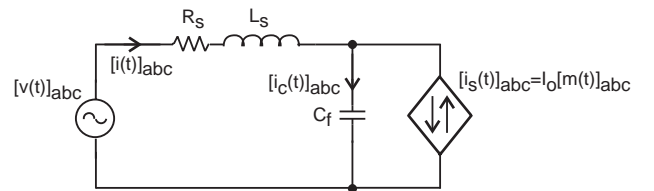


Fig. 6. Per phase equivalent input circuit.

The state equations that represent the above circuit in three-phase coordinates are:

$$[i(t)]_{abc} = [i_c(t)]_{abc} + [i_s(t)]_{abc} \quad (11)$$

$$[i(t)]_{abc} = C_f \cdot \frac{d}{dt} [v_c(t)]_{abc} + [i_s(t)]_{abc} \quad (12)$$

$$[v_c(t)]_{abc} = [v(t)]_{abc} - L_s \cdot \frac{d}{dt} [i_s(t)]_{abc} - R_s \cdot [i(t)]_{abc} \quad (13)$$

Substituting (10) into (12):

$$[i(t)]_{abc} = C_f \cdot \frac{d}{dt} [v_c(t)]_{abc} + I'_o \cdot [m(t)]_{abc} \quad (14)$$

Inserting (13) into (14) results in the input line current of the buck rectifier:

$$[i(t)]_{abc} = C_f \cdot \frac{d}{dt} [v(t)]_{abc} - L_s \cdot C_f \cdot \frac{d^2}{dt^2} [i(t)]_{abc} - R_s \cdot C_f \cdot \frac{d}{dt} [i(t)]_{abc} + I'_o \cdot [m(t)]_{abc} \quad (15)$$

Applying the Park transform to (15) and suppressing the zero sequence coordinate due to the absence of a ground, the main state equations for the *input ac model* in *dqo* coordinates are obtained:

$$\begin{aligned} i_d(t) + R_s \cdot C_f \cdot \frac{di_d(t)}{dt} - \omega R_s \cdot C_f \cdot i_q(t) + L_s \cdot C_f \cdot \frac{d^2 i_d(t)}{dt^2} \\ - 2 \cdot \omega \cdot L_s \cdot C_f \cdot \frac{di_q(t)}{dt} - \omega^2 \cdot L_s \cdot C_f \cdot i_d(t) \\ = C_f \cdot \frac{dv_d(t)}{dt} - \omega \cdot C_f \cdot v_q(t) + m_d(t) \cdot I'_o \end{aligned} \quad (16)$$

$$\begin{aligned} i_q(t) + R_s \cdot C_f \cdot \frac{di_q(t)}{dt} + \omega R_s \cdot C_f \cdot i_d(t) + L_s \cdot C_f \cdot \frac{d^2 i_q(t)}{dt^2} \\ + 2 \cdot \omega \cdot L_s \cdot C_f \cdot \frac{di_d(t)}{dt} - \omega^2 \cdot L_s \cdot C_f \cdot i_q(t) \\ = C_f \cdot \frac{dv_q(t)}{dt} + \omega \cdot C_f \cdot v_d(t) + m_q(t) \cdot I'_o \end{aligned} \quad (17)$$

Using the fundamental concepts of small-signal modeling, linearization and decoupling, in addition to some algebraic manipulations, results in the small-signal transfer function of the *dqo* currents ($\tilde{i}_d(t), \tilde{i}_q(t)$) with respect to the modulation signals ($\tilde{m}_d(t), \tilde{m}_q(t)$) of the *ac input model*:

$$G_i(s) = \frac{\tilde{i}_d(s)}{\tilde{m}_d(s)} = \frac{\tilde{i}_q(s)}{\tilde{m}_q(s)} = \frac{I'_o}{\frac{s^2}{\omega_c^2} + \frac{R_s \cdot s}{L_s \cdot \omega_c^2} + \left(\frac{\omega_c^2 - \omega^2}{\omega_c^2} \right)} \quad (18)$$

B. DC Load Model

In order to obtain a simplified model, the forward/flyback converter is considered to operate as a forward converter in CCM. The flyback sub-converter is neglected because, in this design, the effect of the demagnetizing current is not relevant to the load voltage composition.

The output filter and load are referred to the primary of the transformer and a load equivalent circuit is defined in Figure 7.

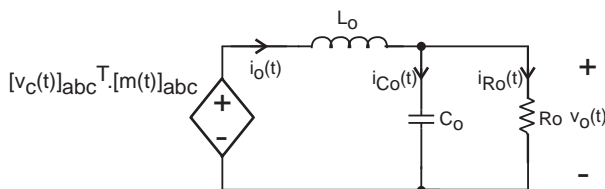


Fig. 7. Load equivalent circuit.

The equations that represent the circuit of Figure 7 are defined below:

$$[v_c(t)]_{abc}^T \cdot [m(t)]_{abc} = L'_o \cdot \frac{di'_o(t)}{dt} + v'_o(t) \quad (19)$$

$$i'_o(t) = C'_o \cdot \frac{dv'_o(t)}{dt} + \frac{v'_o(t)}{R'_o} \quad (20)$$

In this analysis it is considered that the filter capacitor voltage $[v_c(t)]_{abc}$ is in phase with and has the same amplitude as the grid voltage $[v_g(t)]_{abc}$, so that (19) can be rewritten as:

$$[v(t)]_{abc}^T \cdot [m(t)]_{abc} = L'_o \cdot \frac{di'_o(t)}{dt} + v'_o(t) \quad (21)$$

Inserting (20) into (21) yields:

$$[v(t)]_{abc}^T \cdot [m(t)]_{abc} = L'_o \cdot C'_o \cdot \frac{dv_o'^2(t)}{dt^2} + \frac{L'_o}{R'_o} \cdot \frac{dv'_o(t)}{dt} + v'_o(t) \quad (22)$$

In order to obtain a load model in the *dqo* coordinates system the Park transform is applied to (22) and the left-hand terms are defined by the following equality:

$$[v(t)]_{abc}^T \cdot [m(t)]_{abc} = \sqrt{\frac{3}{2}} \cdot \begin{bmatrix} 0 \\ V_{pk} \\ 0 \end{bmatrix}^T \cdot \begin{bmatrix} m_o(t) \\ m_d(t) \\ m_q(t) \end{bmatrix} \quad (23)$$

$$\sqrt{\frac{3}{2}} \cdot V_{pk} \cdot m_d(t) = L'_o \cdot C'_o \cdot \frac{dv_o'^2(t)}{dt^2} + \frac{L'_o}{R'_o} \cdot \frac{dv'_o(t)}{dt} + v'_o(t) \quad (24)$$

The linearized small-signal representation of (25) in the frequency domain is:

$$\sqrt{\frac{3}{2}} \cdot V_{pk} \cdot \tilde{m}_d(s) = L'_o \cdot C'_o \cdot \tilde{v}'_o(s) \cdot s^2 + \frac{L'_o}{R'_o} \cdot \tilde{v}'_o(s) \cdot s + \tilde{v}'_o(s) \quad (25)$$

Substituting the term $\tilde{m}_d(s)$ in (25) by the transfer function of (18), the transfer function of the load voltage $\tilde{v}'_o(s)$ with respect to the direct input current $\tilde{i}_d(s)$ is defined as:

$$G_v(s) = \frac{\tilde{v}'_o(s)}{\tilde{i}_d(s)} = \sqrt{\frac{3}{2}} \cdot \frac{V_{pk}}{I'_o} \cdot \frac{\frac{s^2}{\omega_c^2} + \frac{R_s \cdot s}{L_s \cdot \omega_c^2} + \left(\frac{\omega_c^2 - \omega^2}{\omega_c^2} \right)}{L'_o \cdot C'_o \cdot s^2 + \frac{L'_o}{R'_o} \cdot s + 1} \quad (26)$$

where:

$$\omega_c^2 = \frac{1}{L_s \cdot C_f} \quad (27)$$

C. Closed-Loop Control

The block diagram depicted in Figure 8 comprises the isolated buck rectifier, the coordinate transformations, the modulation and the closed loop load voltage.

The loop control is illustrated in detail in Figure 9, where $C_i(s)$ is the current compensator, $C_v(s)$ is the voltage compensator, K_i is the input current sample gain, K_v is the load voltage sample gain, and V_t^{-1} is the gain that represents the PWM modulator.

In order to control the second-order characteristics of the ac-input, $G_i(s)$, and the dc-load, $G_{vd}(s)$, linear analog compensators were designed.

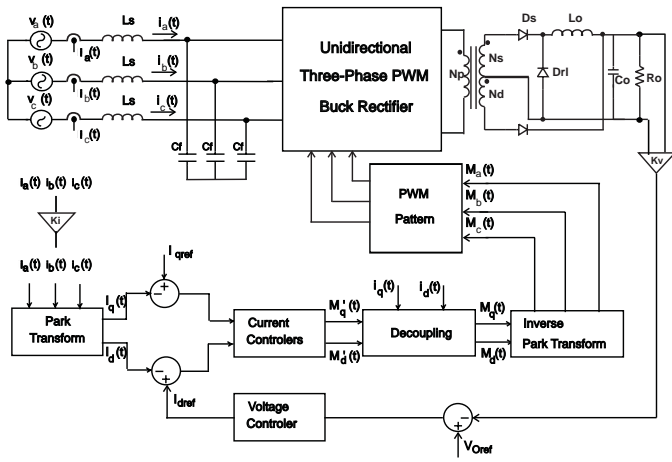


Fig. 8. Complete control loop block diagram.

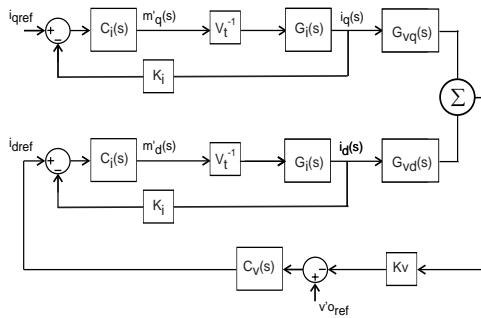


Fig. 9. Complete block diagram of the control loops.

V. SIMULATION RESULTS

In order to validate the proposed isolated buck rectifier, a closed-loop simulation was realized with the following project parameters: $V_{line-line} = 380V$; $f_c = 30kHz$; $P_o = 6kW$; $V_o = 60V$; $I_o = 100A$.

An appropriate design of the ac input filter was carried out to provide a high power-factor (e.g. greater than 0.98), and low T.H.D of line current, (i.e., up to 5%) and resulted in $L_s = 175\mu H$ and $C_f = 23\mu F$.

The transformer, output filter and load parameters are: $L_{mag} = 3.3mH$; $n_p = 28turns$; $n_s = 12turns$; $n_d = 3turns$; $L_o = 130\mu H$; $C_o = 3000\mu F$; $R_o = 0.6\Omega$.

The high quality of the filtered line current is verified in Figure 10. Figure 11 shows the current and voltage waveforms of the ac filter capacitor. Note that the voltage closely follows the grid phase voltage.

The voltage across the secondary diodes can be observed in Figure 12, where the peak values follow the peak voltage values estimated by equations (3), (4) and (5). Figure 13 shows that the core is completely demagnetized by the demagnetization winding. The peak voltage across the switches (see Figure 14) is limited to $\frac{n_p}{n_d} \cdot V_o = 560V$.

The performance of the control system was tested for a 50% load increase. The results of Figure 15 and 16 showed that the voltage was properly controlled

To confirm the excellent performance of the isolated buck rectifier, partially due to the modulation strategy and input filter quality, Figure 17 illustrates the spectrum of the filtered

line current and the total harmonic distortion (THD), which was less than 4%.

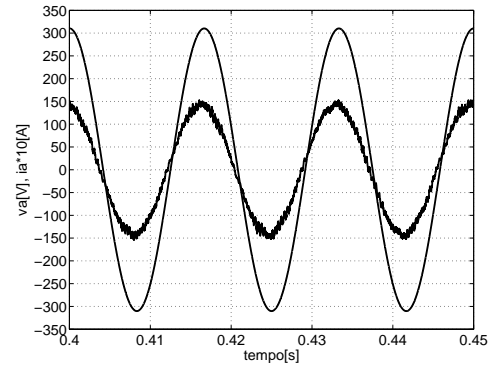


Fig. 10. Phase voltage and line current.

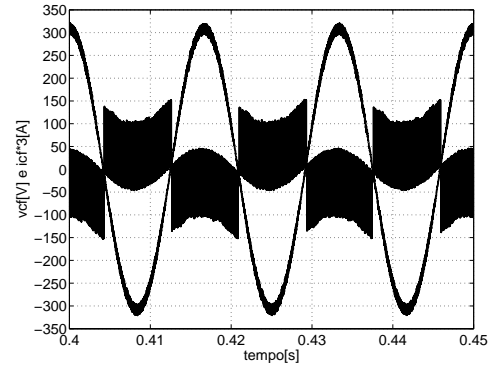


Fig. 11. Voltage and current of ac filter capacitor C_f .

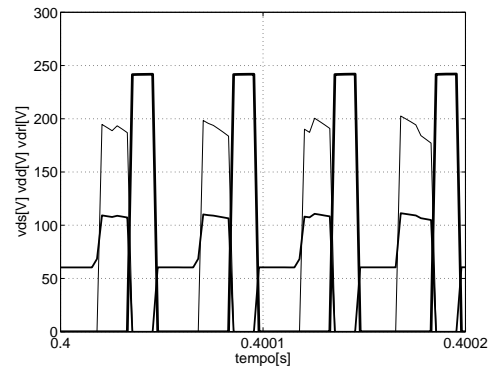


Fig. 12. Voltage across diodes D_s (thick line), D_d and $D_{r,l}$ (thin line).

VI. CONCLUSION

A new single-stage high-frequency isolated three-phase AC/DC converter was presented. The topology uses only three switches and is a promising alternative solution for commercial applications, such as telecommunication power supplies or UPS systems.

The use of the forward/flyback converter is an original, robust and flexible structure to isolate buck rectifiers without using complicated PWM modulation strategies or additional

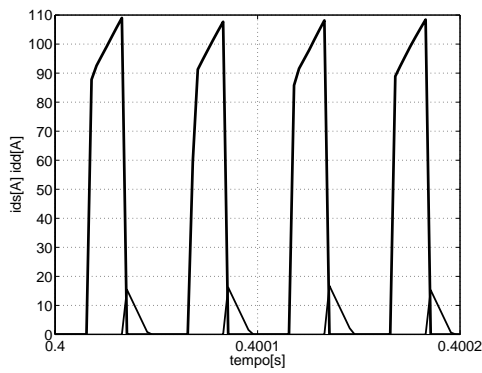


Fig. 13. - Current through diodes D_s and D_d .

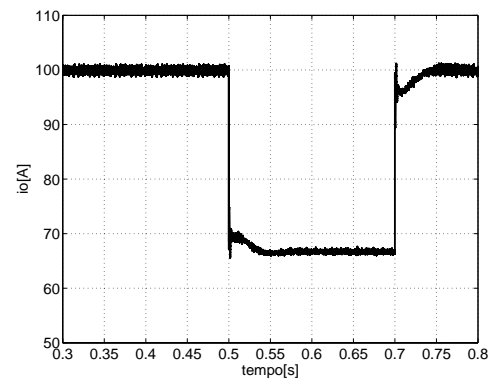


Fig. 16. Load current for a 50% step increase in R_o .

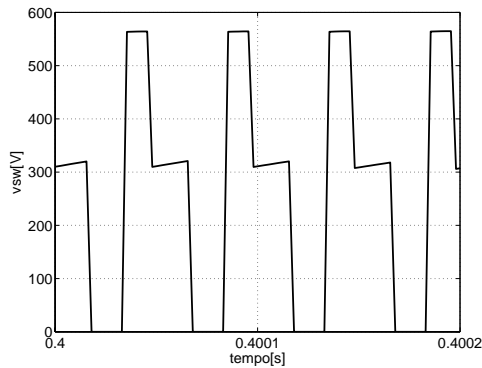


Fig. 14. Voltage across switch S_a .

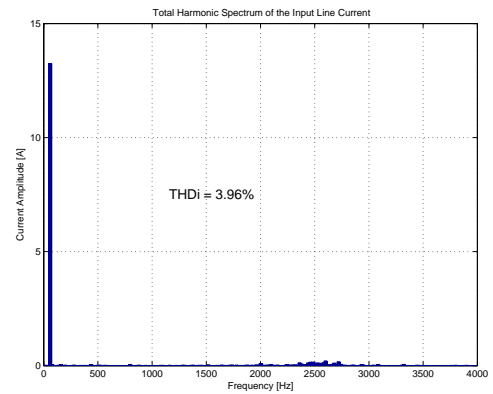


Fig. 17. THD and input line current harmonic spectrum.

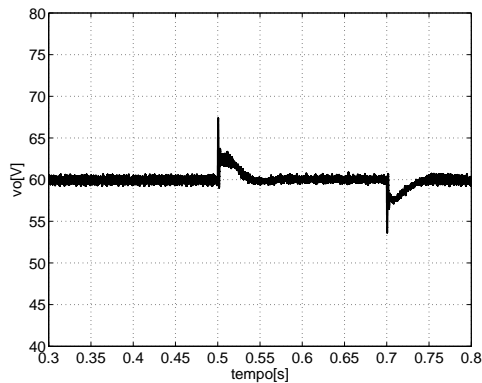


Fig. 15. Load voltage for a 50% step increase in R_o .

switches. The control is based on sampling the input currents and the load voltage, instead of the technique normally used which consists of the additional measuring the voltages across the capacitors.

The transformer is designed to operate over a wide range of turns ratios by using one or more associated transformers. However, special care should be taken with the voltages across the secondary diodes. If these voltages are too high, the feasibility of forward/flyback converter would not be viable.

The new topology was verified by simulations with excellent results. In the near future, results of a prototype that is currently being designed and constructed will be published.

REFERENCES

- [1] Manias, S.; Ziogas, P. D., *A Novel Sinewave in AC to DC with High-Frequency Transformer Isolation*, IEEE Transactions on Industry Electronics, Vol. IE-32, No.4, pp. 430-438, 1985.
- [2] Inagaki, K.; Furuhashi, T.; Ishiguro, A.; Ishida, M.; Okuma, S., *A new PWM control method for ac to dc converters with high-frequency transformer isolation*, IEEE Industry Application Society Conference Proc. 1989, pp. 783-789.
- [3] Vlatkovic, V.; Borojevic, B.; Lee, F. C., *A Zero-Voltage Switched, Three-Phase Isolated PWM Buck Rectifier*, IEEE Transactions on Power Electronics, Vol.10, No.2, March 1995.
- [4] Park, J.N.; Zaloum, T.R., *A Dual Mode Forward/Flyback Converter*, IEEE Power Electronics Specialists Conference, PESC'82 Record, 1982, pp. 3-13.
- [5] Malesani, L.; Tenti, P., *Three-Phase AC/DC PWM Converter with Sinusoidal AC Currents and Minimum Filter Requirements*, IEEE Transactions on Industry Applications, Vol. IA-23, No.1, January/February 1987.
- [6] Wang, X.; Boon-Teck, O., *Unity PF Current-Source rectifier Based on Dynamic Trilogic PWM*, IEEE Transactions on Power Electronics, Vol.8, No.3, July 1993.
- [7] Borgonovo, D., *Modelagem e Controle de Retificadores PWM Trifasicos Empregando a Transformao de Park*, Federal University of Santa Catarina, Master Thesis, Florianopolis, 2001.
- [8] Hiti S.; Vlatkovic V.; Borojevic D.; Lee F.C.Y., *A new control algorithm for three-phase PWM buck rectifier with input displacement factor compensation*, IEEE Transactions on Power Electronics, Vol.9, No.2, pp. 173 - 180, March 1994.
- [9] Espinoza J.R.; Joos G., *State variable decoupling and power flow control in PWM current-source rectifiers*, IEEE Transactions on Industrial Electronics, Vol.45, No.1, pp. 173 - 180, February 1998.